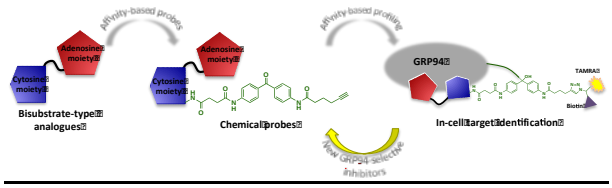
Bisubstrate-type chemical probes identify GRP94 as a potential target of cytosine-containing adenosine analogs.

Dany Pechalrieu[a], Fanny Assemat[a], Ludovic Halby[a,b], Marlene Marcellin[c], Pengrong Yan[d], Karima Chaoui[c], Sahil Sharma[d], Gabriela Chiosis[d], Odile Burlet-Schiltz[c], Paola B. Arimondo[a,b]* and Marie Lopez[a,e]*

[a] ETaC, CNRS FRE3600, Centre de Recherche et Développement Pierre Fabre, Toulouse, France
[b] EpiCBio, Epigenetic Chemical Biology, Department Structural Biology and Chemistry, Institut Pasteur, CNRS UMR n°3523, 28 rue du Dr Roux, 75015 Paris, France
[c] Institut de Pharmacologie et de Biologie Structurale, IPBS, Université de Toulouse, CNRS, UPS, Toulouse, France
[d] Program in Chemical Biology, Memorial Sloan Kettering Cancer Center, New York, New York
[e] Institut des Biomolécules Max Mousseron (IBMM), CNRS, Univ Montpellier, ENSCM UMR 5247, 240 avenue du Prof. E. Jeanbrau, 34296 Montpellier cedex 5, France

* correspondence should be addressed to: Dr. Marie Lopez, IBMM CNRS, email: marie.lopez@cnrs.fr and Dr. Paola B. Arimondo, EpiCBio Institut Pasteur - CNRS, email: paola.arimondo@pasteur.fr

GRAPHICAL ABSTRACT



ABSTRACT

We synthesized affinity-based chemical probes of cytosine-adenosine bisubstrate analogues and identified several potential targets by proteomic analysis. The validation of the proteomic analysis identified the chemical probe as a specific inhibitor of glucose-regulated protein 94 (GRP94), a potential drug target for several types of cancers. Therefore, as a result of the use of bisubstrate-type chemical probes and a chemical-biology methodology, this work opens the way to the development of a new family of GRP94 inhibitors that could potentially be of therapeutic interest.

KEY WORDS

Adenosine-cytosine analogues; chemical probes; affinity-based protein profiling (ABPP); heat shock protein 90 (HSP90); GRP94 inhibitors

INTRODUCTION

Bisubstrate-type enzyme inhibitors consist in the association of two distinct substrate derivatives of an enzyme within the same molecule. In a previous work, we synthesized a library of molecules containing the adenosine motif, present in the SAM (*S*-adenosyl-L-methionine) cofactor of methyltransferases, bound to cytosine analogues to target DNA methyltransferases (DNMTs).[1] Surprisingly, this class of compounds appeared to target protein (*i.e.* histone) arginine methyltransferases (PRMTs).[2] Here, in order to better understand the mode of action of these bisubstrate-type enzyme inhibitors we used both conjugates **1** and **2** (FIG.1), inactive against DNMT, PRMT and histone-lysine *N*-methyltransferases (KHMT), as a starting point to synthesize chemical probes in order to identify their cellular target using affinity-based protein profiling (ABPP) approach.[3, 4] In this strategy, appropriate chemical probes are used to pull-down the protein targets they bind. We chose to incorporate a photoreactive moiety to ensure a covalent crosslink between the chemical probe and protein target. The chemical probes consist of *(i) an affinity moiety (e.g. inhibitor)* to bind to the target protein, (*ii) a photoreactive group* to trap the complexes in the cells upon irradiation and (*iii) a reactive entity* to label and purify the complexes. The key feature consists of using "click chemistry" to label the chemical probe with a fluorescent or affinity tag. We used copper (I)-catalyzed azide-alkyne cycloaddition (CuAAC) as "click reaction" to tag our probes with biotin and purify the associated proteins.[5]

To this aim, we designed a chemical probe derived from the adenosine-cytosine scaffold common to compounds **1** and **2** bearing a benzophenone and an alkyne moiety (compound **4**, FIG.1) and an inactive probe containing the probe reactive scaffold (in green) coupled to a Boc protecting group (compound **5**, FIG .1). Five cancer cell lines were treated with the chemical probe, followed by UV irradiation of the cells to initiate crosslinking and a click reaction was then carried out on the cellular extracts to visualize and pull-down the proteins and analyze them by mass spectrometry. A clear protein pattern was observed and the proteomic analysis results identified glucose-regulated protein 94 (GRP94), a chaperone protein, as a potential target. This is not surprising since the adenosine motif is present in the ATP (adenosine triphosphate) cofactor of GRP94. We then validated GRP94 as a target, thus identifying the adenosine-substituted cytosine scaffold as a starting point for novel inhibitors of this family of molecular chaperones.

RESULTS

In our quest for transition state analogues of DNMTs, we synthesized a chemical library of adenosine-cytosine conjugates. Two conjugates (compounds **1** and **2**), inactive against DNMT, KHMTs and PRMTs (supporting information GRAPH SI-1) are depicted in FIGURE 1 together with the intermediate **3**, the corresponding chemical probe **4** and the probe **5** as control.

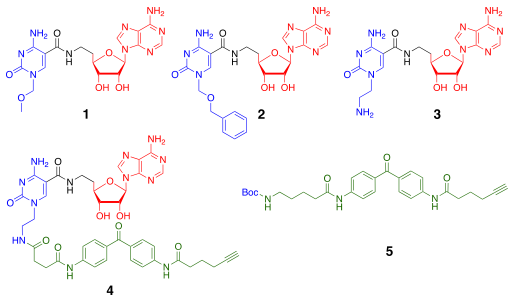
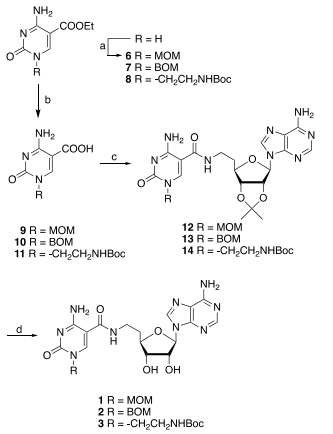


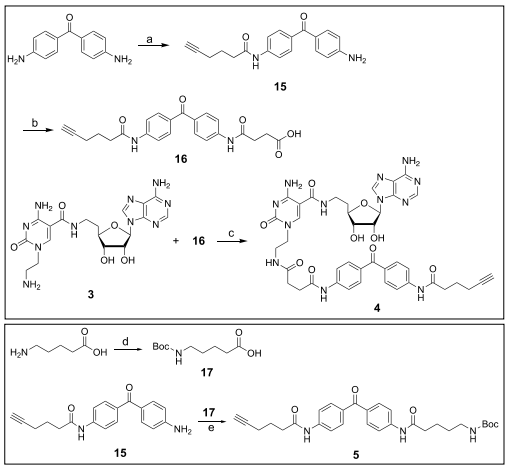
Figure 1. Structure of the compounds **1**-**3** with the adenosine motif (red) linked to the 5-position of the cytosine analogue (blue). Structure of the chemical probes **4** and **5** containing the probe reactive scaffold (green).

Chemical synthesis

Synthesis of the adenosine-cytosine analogues **1-3** (SCHEME 1) started from the ethyl cytosine-5-carboxylate prepared according to the reported literature.[6, 7] The ethyl cytosine-5-carboxylate was then *N*-alkylated with MOM, BOM or Boc-aminoethyl groups to afford compounds **6-8**, respectively. The ester group was then hydrolyzed under basic conditions to afford the carboxycytosine derivatives **9-11**. The carboxylic acids **9-11** were coupled to 2',3'-*O*-isopropylidene-5'-deoxy-5'-aminomethyldenosine [8] to provide the amide derivatives **12-14** and the target compounds **1-3** after deprotection.



Scheme 1. Synthesis scheme of the adenosine-cytosine derivatives **1-3**.
a) MOMCl or BOMBr, Boc-aminoethyl bromide, K_2CO_3, DMF, RT, 18h; b) NaOH, MeOH/H_2O, RT, 12h; c) 2',3'-*O*-isopropylidene-5'-deoxy-5'-aminomethyladenosine, HATU, DIPEA, DMF, RT, 2h; d) TFA, H_2O, RT, 1h.



Scheme 2. Synthetic scheme for chemical probe **4** (upper box) and control probe **5** (bottom box).
a) 5-Hexynoic acid, HATU, DIPEA, DMA, RT, 2h; b) Succinic anhydride, dioxane, 80 °C, 4h; c) HATU, DIPEA, DMF, RT, 16h; d) Di-*tert*-butyl dicarbonate, NaOH, H_2O, dioxane, RT, 16h; e) HATU, DIPEA, DMA, RT, 16h.

The synthesis of chemical probe **4** is presented in SCHEME 2. First, mono-functionalization of the diamino-benzophenone was achieved using HATU as a coupling reagent and 5-hexynoic acid to yield compound **15**. A small linker was then added on the second primary amine of the benzophenone following lactone ring opening with succinic anhydride, which afforded disubstituted benzophenone **16**. The last step involved the coupling of the adenosine-based compound **3** with the benzophenone derivative **16** using HATU as a coupling reagent.

The control probe **5** was synthesized using the alkynylated benzophenone **15** and the Boc-protected 5-aminopentanoic acid **17** (SCHEME 2). The Boc group in control probe **5** was kept for in-cell experiments in order to enable cell permeability.

ABPP experiments

For the gel-based experiments, breast cancer MCF-7 cells were first treated with increasing concentrations of the probe **4**. This was followed by UV irradiation to allow covalent binding of the benzophenone moiety of **4** to the surrounding proteins, leading to an irreversible binding of the probe to the potential protein targets. After cell lysis, the probe was then reacted with TAMRA-biotin-azide through CuAAC, separated by SDS-PAGE, and visualized by in-gel fluorescence scanning to observe the proteins bound to the probe (FIG. 2A AND 2B). We observed an increase in the labeled protein level from 1 to 50 μM of **4** with a highly intense band around 100 kDa. Total protein staining with SYPRO Ruby was used as loading control (FIG. 2B AND 2C lower panel).

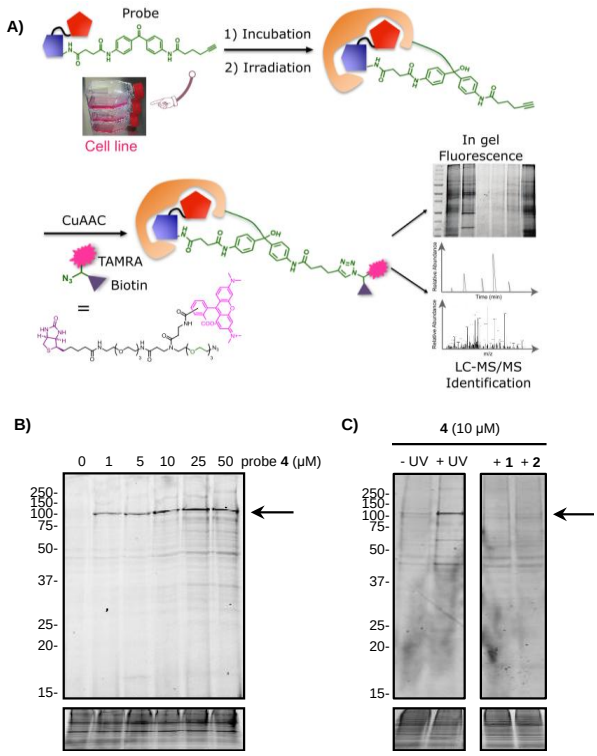


Figure 2. (A) Representation of the general strategy for target identification by using a chemical probe. (B-C) TAMRA fluorescence (upper gels) and SYPRO Ruby stained total protein (bottom gels) profiles of MCF-7 cells treated with a concentration range of probe **4** (B) or with 10 μM of **4** with and without UV irradiation (left) or after competition experiments with 100 μM of competitors **1** and **2** (right) (C).

A 10 μM probe concentration was chosen for the following experiments because the best ratio between fluorescence intensity of the band at 100 kDa over the background was obtained at this concentration when compared to 25 or 50 μM. As expected, in the absence of irradiation, only a weak non-specific fluorescence was detected with no intense band at 100 kDa (FIG. 2C LEFT). To confirm that the labeling is a consequence of recognition of the bisubstrate moiety, we performed competition experiments by adding 100 μM of compound **1** or **2** to the MCF-7 cell culture prior to treatment with the chemical probe **4**. Under these conditions, labeling of probe **4** was completely abolished by

competition with the free compounds **1** and **2** (FIG. 2C RIGHT), which confirm that labeling is due to the affinity of the bisubstrate moiety for this target.

Considering these promising results in MCF-7 cells, other cancer cell lines, *i.e.* leukemia cell lines K-562, KG-1 and MOLM-13, and melanoma cell line WM-266-4, were likewise treated in triplicate with probe **4** (FIG. 3). Similar to that observed in MCF-7 cell line, a band at 100 kDa was strongly labeled in each of these cell lines. Additionally, other significant bands were observed at about 75 and 50 kDa for K-562, KG-1 and WM-266-4 and about 50 and 37 kDa for K-562, KG-1 and MOLM-13. DMSO and probe **5** controls were also analyzed by SDS-PAGE and the absence of fluorescent labeling was confirmed under these conditions (two examples are shown in FIG. 3 right panels). As previously, total protein staining with SYPRO Ruby was used as loading control (FIG. 3 lower panel).

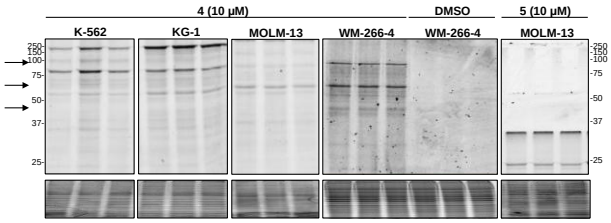


Figure 3. TAMRA fluorescence (upper gels) and total protein staining with SYPRO Ruby stain (bottom gels) after affinity-based profiling in K-562, KG-1, MOLM-13 and WM-266-4 cells upon 1h treatment by 10 µM of probe **4**, control probe **5** or 1% DMSO in triplicate.

Encouraged by these gel-based experiments, we next performed affinity-based pull-down experiments in order to identify the protein targets of the transition state analogue probe **4**. The experiments were performed in three biological replicates in MCF-7, K-562, KG-1, MOLM-13 and WM-266-4 cell lines. The active chemical probe **4** was compared to the inactive Boc probe **5**.

After probe treatment, UV irradiation and CuAAC functionalization of the probe using the trifunctional compound TAMRA-biotin-azide, probe-bound proteins were enriched with avidin beads. After several washings, proteins were trypsin-digested and peptides subjected to LC-MS/MS analysis.

Proteomic analysis

To identify the potential protein targets, quantitative proteomic analysis was carried out on ABPP samples obtained using chemical probe **4** and control probe **5**. The Volcano plot reporting the comparison results is presented in FIGURE 4 for KG-1 cell line and in supplementary information for the other cell lines, *i.e.* MCF-7, K-562, MOLM-13 and WM-266-4 cell lines (GRAPH SI-2 to 5). For KG-1 cell line, about 540 proteins were identified. However as expected, only 24 proteins were found statistically over-represented (*i.e.* Log difference >1 or ratio >2 and -Log 10 p-value >1.33) when the active probe **4** was compared to the inactive probe **5** containing only the Boc moiety (FIG. 4 and TABLE SI-1).

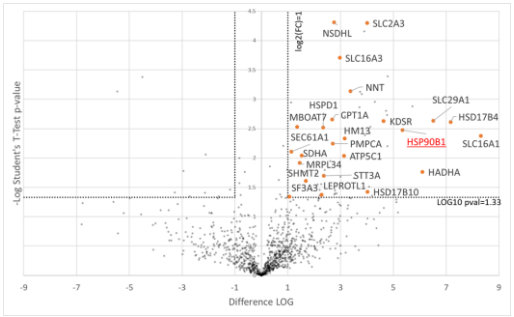
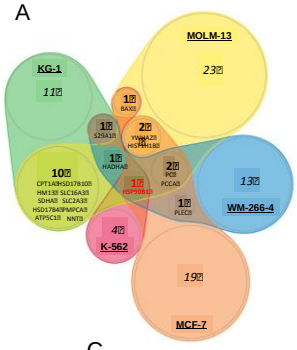


Figure 4. Volcano plot of the proteomic data obtained following pull-down ABPP experiments with active chemical probe **4** and inactive probe **5** in KG-1 cells. The statistical significance expression level change (*p*-value) is represented as a function of the protein ratio between control and treated samples. Orange dots represent the proteins with significantly over-represented in the treated sample.

For the other cell lines 165, 112, 401 and 213 proteins were identified with 26, 6, 40 and 19 statistically over-represented in MCF-7, K-562, MOLM-13 and WM-266-4 cell lines, respectively (GRAPH SI-2 to 5 and TABLE SI-2 to 5)

The different data sets from the five cell lines analyzed were then compared. A Venn diagram analysis revealed that, several proteins were significantly enriched in at least 3 cell lines (FIG. 5A and B, TABLE SI-1 to 5).

A



B

Gene	Cell lines: K-562	KG-1	MOLM-13	WM-266-4	MCF7
BAX					
YWHAZ					
HIST1H1B					
PLEC					
CPT1A					
HM13					
SDHA					
HSD17B4					
ATP5C1					
HSD17B10					
SLC16A3					
SLC2A3					
PMPCA					
NNT					
S29A1					
HADHA					
PC					
PCCA					
HSP90B1					

C

Gene	Protein	Mw (kDa)	Probe 4/Probe 5 ratio*	MS/MS count Probe 5*	MS/MS count Probe 4*
HSP90B1	GRP94	92.468	KG-1 cell line		
			40.61	7	134
			MCF-7 cell line		
			3.78	7	12
			K-562 cell line		
			18.22	7	26
			MOLM-13 cell line		
			16.87	7	35
			WM-266-4 cell line		
			18.74	7	26

Figure 5. Significantly over-represented proteins with chemical probe **4**. (A) Venn diagram showing the common and unique proteins statistically over-represented with the active probe **4** compared to the inactive probe **5**. (B) Table of commonly enriched proteins represented by green highlight in different cell lines. (C) MS/MS counts and ratio values for GRP94 in KG-1, MCF-7, K-562, MOLM-13 and WM-266-4 cell lines. *Ratio values are reported as a mean of the three replicates.

Among these proteins, HSP90B1, also known as GRP94 (M_w= 92 kDa), is the only protein found as significantly enriched in all cell lines with high ratios and abundances in probe **4** treated samples compare to the inactive Boc-containing probe **5** (FIGURE 5 A and C). Therefore, GRP94 represents a promising target of our active chemical probe.

Target validation

To assess the specificity and the binding property of our probe with GRP94, fluorescence polarization competition assays with recombinant GRP94 and HSP90α were performed under conditions of equilibrium binding (FIG. 6).[9] As controls, PU-H71, which is a pan-HSP90 inhibitor under conditions of equilibrium binding but kinetically selects HSP90 residing in epichaperome networks,[10-15] and PU-WS13, which is selective for GRP94 over other isoforms of HSP90,[16-18] were used and showed sub-micromolar EC_{50}s, as previously described.[18] Interestingly, the EC_{50} binding of probe **4** is approximately 10 μM for GRP94 and shows no significant binding to HSP90α up to 50 μM, the highest concentration tested. This assay allows us to confirm that our probe binds to GRP94 specifically compared to HSP90α, confirming the proteomic data and gels. We also assessed compounds **1** and **2** from which the chemical probe was derived. Although both compounds **1** and **2**

showed minor binding to GRP94 at 50 μM, no significant binding to HSP90α was observed at this concentration. Therefore, the absence of the large benzophenone-containing moiety led to a lower inhibition potency but the GRP94 selectivity is maintained for compounds **1** and **2**.

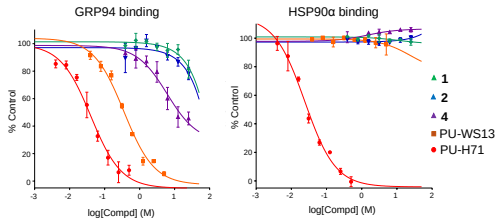


Figure 6. Fluorescence polarization competition assay for GRP94 (left) and HSP90α (right) performed under conditions of equilibrium binding. Binding properties of **4**, **1** and **2** were assessed and PU-H71 and PU-WS13 were included as controls. Data are the mean value of two independent experiments run in triplicates (SD are shown as error bars).

DISCUSSION

Here we applied the ABPP strategy using a chemical probe derived from adenosine-cytosine conjugates to identify potential binding proteins. Since compounds **1** and **2** have no activity on DNMT, HMTs and PRMTs, we were interested in synthesizing a chemical probe from them to use as bait to trap proteins that bind by the APBB strategy. Chemical probe **4** was synthesized and after incubation with five cancer cell lines, the in-cell UV-crosslinked proteins were labeled following click chemistry with the fluorescent TAMRA for visualization and biotin for affinity purification. The TAMRA label revealed, by SDS PAGE, a clear protein-labeling profile, with a common band around 100 kDa. The proteins crosslinked by probe **4** in the five cancer cell lines were analyzed by quantitative proteomics in comparison to the control probe **5** lacking the affinity moiety and with DMSO. The proteomic data analysis showed that, in all tested cancer cell lines, the ATP-binding molecular chaperone GRP94, of the HSP90 family, was selectively labeled by the chemical probe **4** over the DMSO control and control probe **5**. Its detection level was significant and its molecular weight is consistent with the 100-kDa band observed in SDS-PAGE. Additionally, equilibrative nucleoside transporter SLC29A1 (ENT1), hydroxyacyl-CoA dehydrogenase trifunctional multienzyme complex subunit alpha (HADHA), pyruvate carboxylase (PC) and propionyl-CoA carboxylase (PCCA) were also identified by proteomic analysis across at least three cell lines (Figure 5B). SLC29A1 mediates cellular uptake of nucleosides and possess a high affinity for adenosine, chemical moiety present in chemical probe **4**.[19] Its activity is inhibited by anticancer agents (dipyridamole and dilazep) [20] and in leukemia, a down regulation of *SLC29A1* expression, due to a decrease in H3K27 acetylation, was observed in AraC-resistant cell lines.[21] HADHA catalyzes mitochondrial oxidations producing acetyl-CoA from fatty acids and is a component of RNA silencing machinery.[22] *HADHA* expression level is involved in risk of breast cancer [23] and HADHA has a prognostic value in renal cell carcinoma [24]. PC and PCCA are carboxylases of therapeutic interest since the PC is up-regulated in breast cancer and associated with growth and invasion [25] and PCCA dysfunction leads to severe metabolic disorders [26]. These carboxylases possess ATP and nucleotide binding sites. Their identification is then compatible with the adenosine-cytosine chemical structure of the probe **4**. Despite the interest of these additional targets, GRP94 was selected since its molecular weight is consistent with 100 kDa in-gel observed band. Therefore, further validation experiments were focused on GRP94 and fluorescence polarization experiments confirmed selective binding of probe **4** for GRP94 compared to HSP90α.

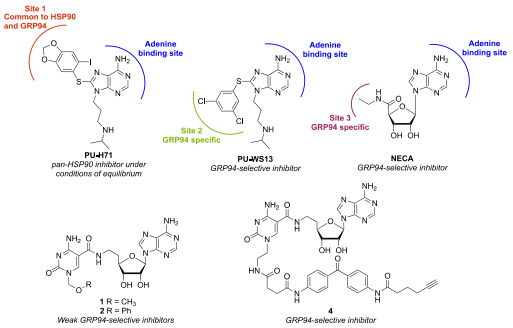


Figure 7. Structures of PU-H71, a pan-HSP90 inhibitor under conditions of equilibrium binding, PU-WS13 and NECA, GRP94-selective inhibitors over HSP90α and HSP90β and compounds **1**, **2** and **4**, new GRP94-selective inhibitors.

GRP94 (encoded by the HSP90β1 gene), belonging to the heat shock protein 90 (HSP90) family, is an essential chaperone that has ATPase activity enabling the folding of target proteins to their active conformation. HSP90s are very promising clinical targets and several clinical trials are ongoing. [17, 27] Contrary to other HSP90 members that are located in the cytoplasm (HSP90α and HSP90β) or the mitochondria (Trap-1), GRP94 resides in the endoplasmic reticulum (ER). GRP94 was shown to be overexpressed in different types of cancers, including breast, colorectal, lung, pancreatic, gastrointestinal cancers and multiple myeloma.[28] The expression of GRP94 is associated with advanced stage, poor survival and cancer growth and metastasis [29-32] and GRP94 was identified as a biomarker of gastrointestinal cancer [33]. GRP94 was also shown to be linked with chemoresistance.[34, 35] All these data provide rationale for the high interest in GRP94 as a therapeutic target for the development of anticancer therapies. However, the selective inhibition of GRP94 is highly complex due to the high conservation of the ATP-binding site. Currently, only a few selective GRP94 inhibitors have been reported,[17, 36] and none have yet reached clinical evaluation. Thus there is a great interest in identifying new chemical scaffolds as starting points for new inhibitors.

In this work we used an innovative in cell ABPP strategy never applied in an HSP90 context. Compared to the other chemical biology methods previously reported to study HSP90 binding properties that used co-immunoprecipitation [37] or on-beads immobilized affinity scaffold,[38, 39] the method reported here is carried out directly in live cells. Thereby, we identified compound **4** as a GRP94-selective inhibitor over HSP90α. For the GRP94 inhibitor PU-WS13, its selectivity is due to the occupation by the substituted phenyl ring of an allosteric pocket (FIG. 7 Site 2), which is not present in HSP90α/β.[18] On the other hand, PU-H71, a pan-HSP90 inhibitor under conditions of equilibrium binding but kinetically selective for HSP90 residing in epichaperome networks, [10] binds to Site 1 present in both HSP90 α/β and GRP94. Our compound **4** bears an adenosine moiety (FIG. 7), shared by GRP94-selective inhibitor NECA,[40] that binds to the ATP binding site. Additionally, NECA was also shown to interact with Site 3 of GRP94.[40, 41] From our results, we showed that the addition of a cytosine substituted with MOM (compound **1)** or BOM (compound **2**) group to the adenosine moiety results in a loss of activity. The bulky substituted cytosine might prevent from interacting within Site 3. However, the cytosine substitution by a large benzophenone-containing linker leads to active and selective GRP94 inhibitor. Thus, the affinity of compound **4** might be due, in addition to the presence of the adenosine moiety, to the flexible and large benzophenone-containing scaffold that could reach to the similar allosteric pocket as for PU-WS13 (Site 2). However, the reasons for the selectivity of **4** are still not clear and will require further investigation.

Therefore, in this study using an innovative in-cell ABPP strategy we identified the adenosine-substituted cytosine analogues as an interesting starting point for further improvement. Crystallographic data could give highly valuable information to improve the potency of our

compounds and afford potent and selective GRP94 inhibitors to be used potentially as therapeutic anticancer agents.

ACKNOWLEDGMENT

This work was supported by PlanCancer2014 France (no. EPIG201401), the Centre national pour la recherche scientifique (CNRS), the research center Pierre Fabre, the Région Occitanie, Toulouse Métropole, FEDER (Fonds Européens de Développement Régional) and the French Ministry of Research (Programme Investissement d'Avenir, Infrastructures Nationales en Biologie et Santé, Proteomics French Infrastructure project, ANR 10-INBS-08). This work was also funded in part by P01 CA186866 and P30 CA008748 (NCI Core Facility Grant). The authors thank T. Taldone (Sloan Kettering Institute) for discussion and proofreading of the manuscript.

CONFLICT OF INTEREST

G.C. has partial ownership in Samus Therapeutics Inc.

METHODS

Chemical Synthesis

All chemicals were purchased from Sigma-Aldrich or Alfa Aesar. PU-H71, PU-WS13 and GM-cy3B were synthesized and characterized as previously reported.[10, 17, 18, 42, 43]

The NMR spectra were recorded on a Bruker Avance II spectrometer equipped with a ^{13}C cryoprobe at 500 MHz for ^{1}H and 125 MHz for ^{13}C; 2D experiments were performed using standard Bruker programs and atoms attribution was performed thanks to 2D correlations. Chemical shifts are given in ppm. Coupling constants J are measured in Hz. Splitting patterns are designed as follows: s, singlet; bs broad singlet; d, doublet; bd, broad doublet; t, triplet; brt, broad triplet; dd, doublet of a doublet; m, multiplet; ddd, doublet of a doublet of a doublet; q, quartet; quint, quintet, sext, sextet.

HRMS-ESI were obtained on a Bruker MicroTOF.

Column chromatography was carried out on a puriflash 430 apparatus (Interchim) equipped with 30 μm porated silica column.

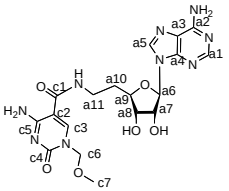
Semi preparative HPLC was performed on an apparatus equipped with a VWR International LaPrep pump P110, a VWR LaPrep P314 Dual l absorbance detector and EZChrom software. C18 reversed-phase column (Waters x-bridge, RP-18, 25 x 250 mm, 5 μm) were used for semi preparative HPLC with a binary gradient elution (solvent A: H_2O/0.01% TEA and solvent B: CH_3CN/0.01% TEA), a flow rate of 20 mL.min^{-1} and the chromatogram was monitored at 250 and 320 nm.

General procedure for synthesis of compounds 1, 2 and 3

Water (100 μl) was added to a solution of **12** (102 mg; 0.20 mmol), **13** (126 mg; 0.22 mmol) or **14** (121 mg; 0.20 mmol) in TFA (1 mL). The reaction mixtures were stirred at room temperature for 1h. The solvent was removed and the residues were co-evaporated three times with 1N ammonia in methanol under reduce pressure. The residues were purified by reversed phase HPLC using a linear gradient H_2O/acetonitrile:100/0→20/80 with 0.2% of TEA to give the desired products.

1-(methoxymethyl)-*N*-((5'-deoxyadenosin-5'-yl)methyl)cytosine-5-carboxamide (1)

Compound **1** was obtained as a white amorphous solid (74 mg; 0.16 mmol; 80%).



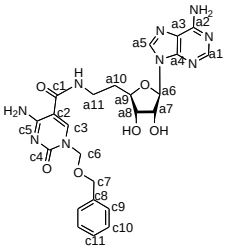
^{1}H NMR (500 MHz, DMSO-*d*$_6$) δ 8.43-8.27 (m, 3H, 1H$_{NH}$, H$_{a5}$, H$_{c3}$), 8.16 (s, 1H, H$_{a1}$), 7.79 (brs, 1H, H$_{NH}$), 7.79 (s, 1H, H$_{NH}$), 7.30 (s, 2H, H$_{NH}$), 5.88 (d, *J*= 5.0 Hz, 1H, H$_{a6}$), 5.49 (d, *J*= 5.8 Hz, 1H, H$_{OH}$), 5.22 (d, *J*= 5.5 Hz, 1H, H$_{OH}$), 5.04 (s, 2H, H$_{c6}$), 4.66 (q, *J*= 5.3 Hz, 1H, H$_{a7}$), 4.10 (q, *J*= 5.4 Hz, 1H, H$_{a8}$), 3.93 (dt, *J*= 4.4, 9.0 Hz, 1H, H$_{a9}$), 3.33-3.29 (m, 1H, H$_{a11}$), 3.28 (s, 3H, H$_{c7}$), 3.24-3.16 (m, 1H, H$_{a11}$), 2.04-1.80 (m, 2H, H$_{a10}$).

^{13}C NMR (125 MHz, DMSO-*d*$_6$) δ 165.3 (C$_{c5}$), 164.5 (C$_{c1}$), 156.5 (C$_{a2}$), 154.5 (C$_{c4}$), 153.1 (C$_{a1}$), 149.8 (C$_{a4}$), 148.4 (C$_{c1}$), 140.3 (C$_{a5}$), 119.6 (C$_{a3}$), 99.1 (C$_{c2}$), 88.1 (C$_{a6}$), 81.0 (C$_{a9}$), 79.6 (C$_{c6}$), 73.8 (C$_{a7}$), 73.5 (C$_{a8}$), 56.7 (C$_{c7}$), 36.4 (C$_{a11}$), 33.4 (C$_{a10}$).

HRMS-ESI (m/z) calculated for $C_{18}H_{24}N_9O_6$ $[M+H]^+$: 462.1844; found: 462.1942.

1-(benzoxymethyl)-*N*-(5'-deoxyadenosin-5'-yl)methyl)cytosine-5-carboxamide (2)

Compound **2** was obtained as a white amorphous solid (96 mg; 0.18 mmol; 81%).



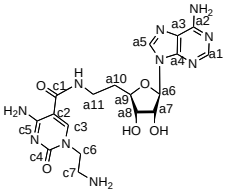
^{1}H NMR (500 MHz, DMSO-*d*$_6$) δ 8.42 (s, 1H, H$_{c3}$), 8.39-8.26 (m, 3H, 2H$_{NH}$ and H$_{a5}$), 8.16 (s, 1H, H$_{a1}$), 7.81 (brs, 1H, H$_{NH}$), 7.39-7.21 (m, 7H, H$_{c9}$, H$_{c10}$, H$_{c11}$, 2H$_{NH}$), 5.88 (d, *J*= 5.0 Hz, 1H, H$_{a6}$), 5.49 (d, *J*= 5.8 Hz, 1H, H$_{OH}$), 5.25-5.16 (m, 3H, H$_{OH}$, H$_{c6}$), 4.66 (ddd, *J*= 5.3, 10.9 Hz, 1H, H$_{a7}$), 4.60 (s, 2H, H$_{c7}$), 4.14-4,08 (m, 1H, H$_{a8}$), 3.94 (dt, *J*= 4.5, 9.1 Hz, 1H, H$_{a9}$), 3.34-3.26 (m, 1H, H$_{a11}$), 3.23-3.18 (m, 1H, H$_{a11}$), 2.01-1.82 (m, 2H, H$_{a10}$).

^{13}C NMR (125 MHz, DMSO-*d*$_6$) δ 163.6 (C$_{c5}$), 160.3 (C$_{c1}$), 152.1 (C$_{a4}$), 150.3 (C$_{c2}$), 149.0 (C$_{a1}$), 148.9 (Ca4), 147.3 (C$_{c3}$), 142.5 (C$_{a5}$), 137.6 (C$_{c8}$), 128.7 (C$_{c10}$), 128.3 (C$_{c11}$), 128.2 (C$_{c9}$), 119.4 (C$_{a3}$), 98.7 (C$_{c2}$), 88.4 (C$_{a6}$), 82.2 (C$_{a9}$), 78.6 (C$_{c6}$), 73.9 (C$_{a7}$), 73.8 (C$_{a8}$), 71.4 (C$_{c7}$), 55.5 (C$_{c7}$), 36.5 (C$_{a11}$), 33.2 (C$_{a10}$).

HRMS-ESI (m/z) calculated for $C_{24}H_{28}N_9O_7$ $[M+H]^+$: 538.2757; found: 538.2161.

1-(2-aminoethyl)-*N*-(5'-deoxyadenosin-5'-yl)methyl)cytosine-5-carboxamide (3)

Compound **3** was obtained as a white amorphous solid (69 mg; 0.15 mmol; 75%).

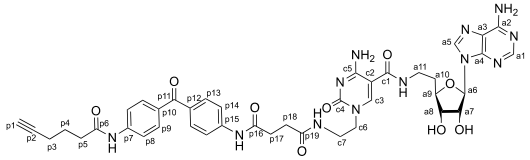


^{1}H NMR (500 MHz, DMSO-d_6) δ 8.35 (s, 1H, H_{c3}), 8.28 (s, 1H, H_{a5}), 8.24 (t, *J*= 5.1 Hz, 1H, H_{NH}), 8.18-8.06 (m, 3H, H_{a1} and $2H_{NH}$), 7.57 (d, *J*= 23.6 Hz, 1H, H_{NH}), 7.30 (s, 2H, H_{NH}), 5.87 (d, *J*= 4.9 Hz, 1H, H_{a6}), 5,65-5,04 (m, 2H, H_{NH}), 4.66 (t, *J*= 5.2 Hz, 1H, H_{a7}), 4.11 (t, *J*= 5.0 Hz, 1H, H_{a6}), 3.94 (tt, *J*= 9.0, 4.3 Hz, 1H, H_{a9}), 3.68 (t, *J*= 6.2 Hz, 2H, H_{c6}), 3.24-3.14 (m, 2H, H, H_{a11}), 2.88-2.70 (m, 2H, H_{c7}), 2.03-1.79 (m, 2H, H_{a10}),

^{13}C NMR (125 MHz, DMSO-d_6) δ 165.7 (C_{c5}), 164.4 (C_{c1}), 156.5 (C_{a2}), 154.7 (C_{c4}), 153.1 (C_{a1}), 149.8 (C_{a4}), 149.7 (C_{a1}), 140.3 (C_{c3}), 119.6 (C_{a3}), 97.8 (C_{c2}), 88.1 (C_{a6}), 81.8 (C_{a9}), 73.8 (C_{a6}), 73.5 (C_{a7}), 52.5 (C_{c6}), 40.5 (C_{c7}), 36.3 (C_{a11}), 33.5 (C_{a10}).

HRMS-ESI (m/z) calculated for $C_{18}H_{25}N_{10}O_5$ $[M+H]^+$: 461.2004; found: 461.2011.

Synthesis of chemical probe 4



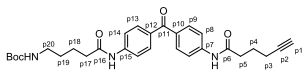
To a solution of 4-((4-(4-(hex-5-ynamido)benzoyl)phenyl)amino)-4-oxobutanoic acid **16** (6.7 mg; 16 μmol), HATU (8 mg; 20 μmol) and DIPEA (7 μl; 38 μmol) in DMF (0.4 mL) was added **3** (6.3 mg; 4 μmol). The mixture was stirred at room temperature for 16 hours. The residue was then directly purified by reversed phase HPLC using a linear gradient H_2O/acetonitrile:100/0→20/80 with 0.01% of TEA to afford **4** as a amorphous white solid (8.3 mg; 9.8 μmol; 72%).

^{1}H NMR (500 MHz, DMSO) δ 10.33 (s, 1H, H_{NH}), 10.30 (s, 1H, H_{NH}), 8.32 (s, 1H, H_{a5}), 8.28 (s, 1H, H_{c3}), 8.24 (brt, 1H, H_{NH}), 8.14 (s, 1H, H_{a1}), 8.08 (brt, 1H, H_{NH}), 7.77-7.71 (m, 4H, H_{p9}, H_{p13}), 7.71-7.66 (m, 4H, H_{p8}, H_{p14}), 7.28 (brs, 2H, H_{NH2}), 5.86 (d, *J*= 5.1 Hz, 1H, H_{a6}), 5.51-5.46 (m, 1H, H_{OH}), 5.24-5.18 (m, 1H, H_{OH}), 4.64 (t, *J*= 4.9 Hz, 1H, H_{a7}), 4.08 (t, *J*= 5.2 Hz, 1H, H_{a8}), 3.98-3.91 (m, 1H, Ha9), 3.72 (t, *J*= 5.9 Hz, 2H, H_{a11}), 3.32-3.26 (m, 3H, H_{c6} and H_{c7}), 3.21-3.12 (m, 1H, H_{c7}), 2.83 (t, *J*= 2.7 Hz, 1H, H_{p1}), 2.61 (t, *J*= 7.0 Hz, 2H, H_{p17}), 2.48 (t, *J*= 7.4 Hz, 2H, H_{p5}), 2.41 (t, *J*= 7.1 Hz, 2H, H_{p18}), 2.24 (dt, *J*= 2.8, 7.3 Hz, 2H, H_{p3}), 1.96-1.81 (m, 2H, H_{a10}), 1.78 (quint, *J*= 7.4Hz, 2H, H_{p4}).

^{13}C NMR (125 MHz, DMSO) δ 193.4 (C_{p11}), 171.6 (C_{p19}), 171.2 (C_{p6}, C_{p16}), 165.2 (C_{c1}), 164.1 (C_{c4}), 156.07 (C_{c5}), 154.1 (C_{a2}), 152.7 (C_{a1}), 149.4 (C_{a4}), 149.0 (C_{c3}), 143.0 (C_{p15}, C_{p7}), 139.8 (C_{a5}), 131.7 (C_{p10} and C_{p12}), 130.9 (C_{p9} and C_{p13}), 119.2 (C_{a3}), 118.2 (C_{p8} and C_{p14}), 97.6 (C_{c2}), 87.7 (C_{a6}), 83.9 (C_{p2}), 81.3 (C_{a9}), 73.4 (C_{a7}), 73.1 (C_{a8}), 71.8 (C_{p1}), 49.2 (C_{a11}), 37.8 (C_{c6}), 35.8 (C_{c7}), 35.2 (C_{p5}), 33.1 (C_{a10}), 31.6 (C_{p17}), 30.0 (C_{p18}), 23.8 (C_{p4}), 17.3 (C_{p3}).

HRMS-ESI (m/z) calculated for $C_{41}H_{45}N_{12}O_9$ $[M+H]^+$: 849.3427; found: 849.3436.

***N*-(4-(4-(5-(Boc-amino)pentanamido)benzoyl)phenyl)hex-5-ynamide (5)**



HATU (396.0 mg; 1.04 mmol) was solubilized in DMA (2 mL) at RT under argon. The carboxylic acid **17** (215.0 mg; 0.99 mmol) and DIPEA (0.19 mL; 1.39 mmol) was added to the solution. After 20 min of stirring at room temperature, the compound **15** (198.9 g; 0.65 mmol) was then added. The reaction mixture was stirred at room temperature for 16 h. The residue was diluted with ethyl acetate and washed with water and brine, and dried over sodium sulfate. The solvent was removed and the

residue was purified by silica gel flash chromatography using a linear gradient of cyclohexane/ethyl acetate:0/100→80/20 to afford the title compound **5** as an amorphous white solid (309.8 mg; 0.57 mmol; 88% yield).

^{1}H NMR (500 MHz, DMSO) δ 10.31 (s, 1H, H_{NH}), 10.25 (s, 1H, H_{NH}), 7.78-7.67 (m, 8H, H_{p8}, Hp9, H_{p13} and H_{p14}), 6.82 (t, *J*= 5.5 Hz, 1H, H_{NH}), 2.93 (q, *J*= 6.5 Hz, 2H, H_{p20}), 2.83 (t, *J*= 2.7 Hz, 1H, H_{p1}), 2.48 (t, *J*= 7.7 Hz, 2H, H_{p5}), 2.35 (t, *J*= 7.5 Hz, 2H, H_{p17}), 2.24 (dt, *J*= 2.5, 7.0 Hz, 2H, H_{p3}), 1.78 (quint, *J*= 7.2 Hz, 2H, H_{p4}), 1.58 (quint, *J*= 7.7 Hz, 2H, H_{p18}), 1.41 (quint, *J*= 7.2 Hz, 2H, H_{p19}), 1.37 (s, 9H, H_{Boc}).

^{13}C NMR (125 MHz, DMSO) δ 193.4 (C_{p11}), 171.8 (C_{p6}), 171.2 (C_{p16}), 155.6 (C_{Boc}), 143.1 (Cp7), 143 (C_{p15}), 131.7 (C_{p10}, C_{p12}), 130.9 (C_{p13}, C_{p9}), 118.2 (C_{p8}, C_{p14}), 84 (C_{p2}), 77.4 (C_{Boc}), 71.7 (C_{p1}), 39.4 (C_{p20}), 36.2 (C_{p17}), 35.2 (C_{p5}), 29.1 (C_{p19}), 28.2 (C_{Boc}), 23.8 (C_{p4}), 22.4 (Cp18), 17.3 (C_{p3}).

HRMS-ESI (m/z) calculated for $C_{29}H_{35}N_3O_5Na$ $[M+Na]^+$: 528.2469; found: 528.2471.

Cell culture

KG-1, MOLM-13 and K-562 human leukemia cell lines, WM-266-4 human melanoma cancer cells and MCF-7 human breast cancer cells were obtained from ATCC (USA). Cells were grown in RPMI 1640 GlutaMAX™ (ThermoFisher Scientific) medium containing 10% FCS (Lonza) for K-562 and MCF-7 cells and 20% for KG-1 and MOLM-13 cells, WM-266-4 cell line was grown in EMEM containing 10% FCS at 37 °C and under 5% CO_2.

***In situ* labeling of cancer cells for in-gel visualization**

For probe labeling assays, suspension cells were counted and adherent cells were grown until approximately 90-80% confluent before treatment. They were first washed twice with PBS and resuspended in their medium without FCS for the incubation with probes. Probe was added at desired concentration and incubated for 1 h at 37 °C. Chemical probe **4** was used for measurement sample and chemical probe **5** was used as control experiments for proteomic analysis. DMSO (1% v/v) was added in control samples. Competitor (**1** or **2)** was added 30 min after the test compound to chase. Following treatment, cells were washed once with PBS and resuspended in fresh medium for the UV-irradiation step. After 1 h of exposition at 365 nm, cells were lysed in lysis buffer (RIPA buffer (Sigma-Aldrich) + cOmplete™, EDTA-free Protease Inhibitor Cocktail (PIC) (Roche Diagnostics)) on ice for 15 min followed by 3 min of sonication (30 s / 30 s on/off, medium power, Diagenode Bioruptor®). Protein concentrations were determined and proteome samples were diluted in PBS at a final concentration of 1 $mg.mL^{-1}$ for the CuAAC ligation. The premix reagents (60 μM TAMRA-biotin-azide, 1 mM $CuSO_4$, 1 mM TCEP and 100 μM TBTA, final concentrations) were added to the lysate. The samples were agitated for 1h at room temperature. The proteins were next precipitated by addition of methanol/chloroform/water (2/0.5/1) and pelleted by centrifugation at 15,000 × g for 5 min. After removal of supernatant, protein pellet was further washed in methanol and resuspended in PBS buffer containing 2% SDS and 10 mM DTT. Läemmli sample buffer was then added and the samples were heated for 10 min at 95 °C, separated by 1D SDS-PAGE and visualized using Typhoon 9410 (GE Healthcare).

***In situ* labeling of cancer cells for gel and MS analysis**

In parallel to SDS-PAGE visualization, samples were enriched on avidin-coupled agarose beads (Pierce™ NeutrAvidin™ Agarose, ThermoFisher Scientific) (50 μL, pre-washed three times in 0.2%

SDS in PBS) by incubation with gentle shaking for 2 h at room temperature to bind and enrich biotin-labeled proteins. The supernatant was then removed and the beads were washed with 1% SDS in PBS (3 x 1 mL), 4 M urea in 50 mM ammonium bicarbonate (AMBIC) (2 x 1 mL) and 50 mM AMBIC (5 x 1 mL).

On-bead proteins were then resuspended in 50 µL of 50 mM AMBIC and reduced with 10 mM dithiothreitol at 55 °C for 30 min. After on-bead reduction, samples were washed twice with 50 mM AMBIC and again resuspended in 50 µL of 50 mM AMBIC for alkylation of cysteines by 10 mM iodoacetamide in the dark for 30 min. Beads were then washed twice with 50 mM AMBIC and resuspended in 50 µl of 50 mM AMBIC for protein digestion with trypsin (1 µg, Promega), overnight at 37 °C. Supernatant was kept in clean Eppendorf and beads were washed with 50 mM AMBIC followed by 0.1% TFA in H_2O. Supernatants of each washing step were combined, evaporated to dryness and resuspended for desalting step before LC-MS/MS analysis.

Peptides were analyzed by nanoLC-MS/MS using an UltiMate 3000 RSLCnano system coupled to an Orbitrap Velos mass spectrometer (Thermo Fisher Scientific, Bremen, Germany). 5 µl of each sample were loaded on a C-18 precolumn (300 µm ID x 5 mm, Thermo Fisher) in water containing 5% acetonitrile and 0.05% TFA and at a flow rate of 20 $\mu L.min^{-1}$. After 5 min of desalting, the precolumn was switched online with the analytical C-18 column (75 µm ID x 50 cm, Reprosil C18) equilibrated in 95% solvent A (5% acetonitrile, 0.2% formic acid) and 5% solvent B (80% acetonitrile, 0.2% formic acid). Peptides were eluted using a 5 to 50% gradient of solvent B over 105 min at a flow rate of 300 $nL.min^{-1}$. The orbitrap Velos was operated in a data-dependent acquisition mode with the XCalibur software. Survey scan MS were acquired in the Orbitrap on the 350-1800 m/z range with the resolution set to a value of 60000. The 20 most intense ions per survey scan were selected for CID fragmentation. Dynamic exclusion was employed within 60s to prevent repetitive selection of the same peptide.

Raw mass spectrometry files were processed with the MaxQuant software (version 1.5.2.8) for database search with the Andromeda search engine and quantitative analysis. Data were searched against human entries of the Swissprot protein database. Carbamidomethylation of cysteines was set as a fixed modification whereas oxidation of methionine and protein *N*-terminal acetylation were set as variable modifications. Specificity of trypsin digestion was set for cleavage after K or R, and two missed trypsin cleavage sites were allowed. The precursor mass tolerance was set to 20 ppm for the first search and 4.5 ppm for the main Andromeda database search. The mass tolerances MS/MS mode was set to 0.5 Da. Andromeda results were validated by the target-decoy approach using a reverse database at both a peptide and a protein FDR of 1%. For label-free relative quantification of the samples, the "match between runs" option of MaxQuant was enabled with a time window of 0.7 min, to allow cross-assignment of MS features detected in the different runs.

Specifically labeled proteins were identified by comparison to the alkyne probe-treated samples with the controls. The "LFQ" metric from the MaxQuant "protein group.txt" output was used and ratio between alkyne probe and controls were calculated. According to different thresholds/filters, proteins were considered specific if ratios are > 2 or Log difference is > 1, Log10 p-value > 1.33, the sum of MS2 count of probe/control > 5 and then if there is a statistically significant difference (Student's t–test, $p = 0.05$).

FP competition assay under conditions of equilibrium binding

The GRP94 and HSP90α FP competition assays were performed on an Analyst GT instrument (Molecular Devices, Sunnyvale, CA) and carried out in black 96-well microplates (Corning, no. 3650)

in a total volume of 100 μL in each well as previously described [9, 44]. A stock of 10 μM Cy3B-GM was prepared in DMSO and diluted with Felts buffer [20 mM HEPES (K) pH 7.3, 50 mM KCl, 2 mM DTT, 5 mM $MgCl_2$, 20 mM Na_2MoO_4, and 0.01% NP40 with 0.1 $mg.mL^{-1}$ BGG]. To each well was added the fluorescent dye labeled ligand (6 nM Cy3B-GM for GRP94 and HSP90α), recombinant protein (10 nM GRP94 or HSP90α) and the tested inhibitor (initial stock in DMSO) in a final volume of 100 μL of Felts buffer. Compounds were added in duplicate wells. For each assay, background wells (buffer only), tracer controls (free, fluorescent dye labeled ligand only), and bound controls (fluorescent dye labeled ligand in the presence of protein) were included on each assay plate. The assay plate was incubated on a shaker at 4 °C for 24 h and the FP values (in mP) were measured. The fraction of fluorescent dye labeled ligand bound to GRP94 or HSP90α was correlated to the mP value and plotted against values of competitor concentrations. The inhibitor concentration at which 50% of bound fluorescent dye labeled ligand got displaced was obtained by fitting the data. For Cy3B-GM, an excitation filter at 530 nm and an emission filter at 580 nm were used with a dichroic mirror of 561 nm. All experimental data were analyzed using SoftMax Pro 6.3 and plotted using Prism 6.0 (Graphpad Software Inc., San Diego, CA) and binding affinity values are given as relative binding affinity values (EC_{50}, concentration at which 50% of fluorescent ligand was competed off by compound). PU-H71 and PU-WS13 were included as controls.

SUPPORTING INFORMATION AVAILABLE

Synthesis and characterization of compounds **6**-**17**. ^{1}H and ^{13}C NMR spectra of compounds **1**-**5**. Inhibition percentages of various DNMT, KHMTs and PRMTs for compounds **1**-**4**. Table of proteomic analysis result tables (Table SI-1 to SI-5) and volcano plot (Graph SI-1 to SI-5). This material is available free of charge *via* the Internet.

References

[1] Halby, L., Menon, Y., Rilova, E., Pechalrieu, D., Masson, V., Faux, C., Bouhlel, M. A., David-Cordonnier, M. H., Novosad, N., Aussagues, Y., Samson, A., Lacroix, L., Ausseil, F., Fleury, L., Guianvarc'h, D., Ferroud, C., and Arimondo, P. B. (2017) Rational design of bisubstrate-type analogs as inhibitors of DNA methyltransferases in cancer cells, *J. Med. Chem. 60*, 4665-4679.

[2] Halby, L., Marechal, N., Pechalrieu, D., Cura, V., Franchini, D.-M., Faux, C., Alby, F., Troffer-Charlier, N., Kudithipudi, S., Jeltsch, A., Aouadi, W., Decroly, E., Guillemot, J.-C., Page, P., Ferroud, C., Bonnefond, L., Guianvarc'h, D., Cavarelli, J., and Arimondo, P. B. (2018) Hijacking DNA methyltransferase transition state analogues to produce chemical scaffolds for PRMT inhibitors, *Philos. Trans. R. Soc. Lond. B Biol. Sci. 373*.

[3] Kawatani, M., and Osada, H. (2014) Affinity-based target identification for bioactive small molecules *MedChemComm 5*, 277-287.

[4] Weigt, D., Hopf, C., and Medard, G. (2016) Studying epigenetic complexes and their inhibitors with the proteomics toolbox, *Clin. Epigenetics 8*, 76.

[5] Sletten, E. M., and Bertozzi, C. R. (2009) Bioorthogonal Chemistry: Fishing for Selectivity in a Sea of Functionality, *Angew. Chem. Int. Ed. 48*, 6974-6998.

[6] Whitehead, C. W. (1953) The Reactions of Orthoesters with Ureas. A New Synthesis of Pyrimidines, *J. Am. Chem. Soc. 75*, 671-675.

[7] Vardanyan, R. S., Hruby, V. J., Danagulyan, G. G., and Mkrtchyan, A. D. (2005) Isomerization/recyclization of some 5- ethoxycarbonyl- pyrimidines, *J. Heterocycl. Chem. 42*, 557-562.

[8] Lerner, C., Masjost, B., Ruf, A., Gramlich, V., Jakob-Roetne, R., Zurcher, G., Borroni, E., and Diederich, F. (2003) Bisubstrate inhibitors for the enzyme catechol-O-methyltransferase (COMT): influence of inhibitor preorganisation and linker length between the two substrate moieties on binding affinity, *Org. Biomol. Chem. 1*, 42-49.

[9] Taldone, T., Patel, P. D., Patel, M., Patel, H. J., Evans, C. E., Rodina, A., Ochiana, S., Shah, S. K., Uddin, M., Gewirth, D., and Chiosis, G. (2013) Experimental and structural testing module to analyze paralogue-specificity and affinity in the Hsp90 inhibitors series, *J. Med. Chem. 56*, 6803-6818.

[10] Rodina, A., Wang, T., Yan, P., Gomes, E. D., Dunphy, M. P. S., Pillarsetty, N., Koren, J., Gerecitano, J. F., Taldone, T., Zong, H., Caldas-Lopes, E., Alpaugh, M., Corben, A., Riolo, M., Beattie, B., Pressl, C., Peter, R. I., Xu, C., Trondl, R., Patel, H. J., Shimizu, F., Bolaender, A., Yang, C., Panchal, P., Farooq, M. F., Kishinevsky, S., Modi, S., Lin, O., Chu, F., Patil, S., Erdjument-Bromage, H., Zanzonico, P., Hudis, C., Studer, L., Roboz, G. J., Cesarman, E., Cerchietti, L., Levine, R., Melnick, A., Larson, S. M., Lewis, J. S., Guzman, M. L., and Chiosis, G. (2016) The epichaperome is an integrated chaperome network that facilitates tumour survival, *Nature 538*, 397.

[11] Joshi, S., Wang, T., Araujo, T. L. S., Sharma, S., Brodsky, J. L., and Chiosis, G. (2018) Adapting to stress - chaperome networks in cancer, *Nat. Rev. Cancer 18*, 562-575.

[12] Kourtis, N., Lazaris, C., Hockemeyer, K., Balandran, J. C., Jimenez, A. R., Mullenders, J., Gong, Y., Trimarchi, T., Bhatt, K., Hu, H., Shrestha, L., Ambesi-Impiombato, A., Kelliher, M., Paietta, E., Chiosis, G., Guzman, M. L., Ferrando, A. A., Tsirigos, A., and Aifantis, I. (2018) Oncogenic hijacking of the stress response machinery in T cell acute lymphoblastic leukemia, *Nat. Med. 24*, 1157-1166.

[13] Kishinevsky, S., Wang, T., Rodina, A., Chung, S. Y., Xu, C., Philip, J., Taldone, T., Joshi, S., Alpaugh, M. L., Bolaender, A., Gutbier, S., Sandhu, D., Fattahi, F., Zimmer, B., Shah, S. K., Chang, E., Inda, C., Koren, J., 3rd, Saurat, N. G., Leist, M., Gross, S. S., Seshan, V. E., Klein, C., Tomishima, M. J., Erdjument-Bromage, H., Neubert, T. A., Henrickson, R. C., Chiosis, G., and Studer, L. (2018) HSP90-incorporating chaperome networks as biosensor for disease-related pathways in patient-specific midbrain dopamine neurons, *Nat. Comm. 9*, 4345.

[14] Taldone, T., Wang, T., Rodina, A., Pillarsetty, N. V. K., Digwal, C. S., Sharma, S., Yan, P., Joshi, S., Pagare, P. P., Bolaender, A., Roboz, G. J., Guzman, M. L., and Chiosis, G. (2019) A Chemical Biology Approach to the Chaperome in Cancer-HSP90 and Beyond, *Cold Spring Harb. Perspect. Biol.*, doi: 10.1101/cshperspect.a034116.

[15] Pillarsetty, N., Jhaveri, K., Taldone, T., Caldas-Lopes, E., Punzalan, B., Joshi, S., Bolaender, A., Uddin, M. M., Rodina, A., Yan, P., Ku, A., Ku, T., Shah, S. K., Lyashchenko, S., Burnazi, E., Wang, T., Lecomte, N., Janjigian, Y., Younes, A., Batlevi, C. W., Guzman, M. L., Roboz, G. J., Koziorowski, J., Zanzonico, P., Alpaugh, M. L., Corben, A., Modi, S., Norton, L., Larson, S. M., Lewis, J. S., Chiosis, G., Gerecitano, J. F., and Dunphy, M. P. S. (2019) Paradigms for Precision Medicine in Epichaperome Cancer Therapy, *Cancer Cell 36*, 559-573 e557.

[16] Shrestha, L., Patel, H. J., and Chiosis, G. (2016) Chemical Tools to Investigate Mechanisms Associated with HSP90 and HSP70 in Disease, *Cell Chem. Biol. 23*, 158-172.

[17] Patel, H. J., Patel, P. D., Ochiana, S. O., Yan, P., Sun, W., Patel, M. R., Shah, S. K., Tramentozzi, E., Brooks, J., Bolaender, A., Shrestha, L., Stephani, R., Finotti, P., Leifer, C., Li, Z., Gewirth, D. T., Taldone, T., and Chiosis, G. (2015) Structure-activity relationship in a purine-scaffold compound series with selectivity for the endoplasmic reticulum Hsp90 paralog Grp94, *J. Med. Chem. 58*, 3922-3943.

[18] Patel, P. D., Yan, P., Seidler, P. M., Patel, H. J., Sun, W., Yang, C., Que, N. S., Taldone, T., Finotti, P., Stephani, R. A., Gewirth, D. T., and Chiosis, G. (2013) Paralog-selective Hsp90 inhibitors define tumor-specific regulation of HER2, *Nat. Chem. Biol. 9*, 677-684.

[19] Tromp, R. A., Spanjersberg, R. F., von Frijtag Drabbe Kunzel, J. K., and IJzerman, A. P. (2005) Inhibition of nucleoside transport proteins by C8-alkylamine-substituted purines, *J. Med. Chem. 48*, 321-329.

[20] Visser, F., Vickers, M. F., Ng, A. M. L., Baldwin, S. A., Young, J. D., and Cass, C. E. (2002) Mutation of residue 33 of human equilibrative nucleoside transporters 1 and 2 alters sensitivity to inhibition of transport by dilazep and dipyridamole, *J. Biol. Chem. 277*, 395-401.

[21] Stief, S. M., Hanneforth, A.-L., Weser, S., Mattes, R., Carlet, M., Liu, W.-H., Bartoschek, M. D., Dominguez Moreno, H., Oettle, M., Kempf, J., Vick, B., Ksienzyk, B., Tizazu, B., Rothenberg-Thurley, M., Quentmeier, H., Hiddemann, W., Vosberg, S., Greif, P. A., Metzeler, K. H., Schotta, G., Bultmann, S., Jeremias, I., Leonhardt, H., and Spiekermann, K. (2020) Loss of KDM6A confers drug resistance in acute myeloid leukemia, *Leukemia 34*, 50-62.

[22] Kakumani, P. K., Shanmugam, R. K., Kaur, I., Malhotra, P., Mukherjee, S. K., and Bhatnagar, R. K. (2015) Association of HADHA with human RNA silencing machinery, *Biochem. Biophys. Res. Commun. 466*, 481-485.

[23] Mamtani, M., and Kulkarni, H. (2012) Association of HADHA expression with the risk of breast cancer: targeted subset analysis and meta-analysis of microarray data, *BMC Res. Notes 5*, 25.

[24] Zhao, Z., Lu, J., Han, L., Wang, X., Man, Q., and Liu, S. (2016) Prognostic significance of two lipid metabolism enzymes, HADHA and ACAT2, in clear cell renal cell carcinoma, *Tumour Biol. 37*, 8121-8130.

[25] Phannasil, P., Thuwajit, C., Warnnissorn, M., Wallace, J. C., MacDonald, M. J., and Jitrapakdee, S. (2015) Pyruvate Carboxylase Is Up-Regulated in Breast Cancer and Essential to Support Growth and Invasion of MDA-MB-231 Cells, *PLoS One 10*, e0129848.

[26] Wongkittichote, P., Ah Mew, N., and Chapman, K. A. (2017) Propionyl-CoA carboxylase - A review, *Mol. Genet. Metab. 122*, 145-152.

[27] Xiao, Y., and Liu, Y. (2019) Recent Advances in the Discovery of Novel HSP90 Inhibitors: An Update from 2014, *Curr. Drug Targets 21*, 302-317.

[28] Lee, A. S. (2014) Glucose-regulated proteins in cancer: molecular mechanisms and therapeutic potential, *Nat. Rev. Cancer 14*, 263-276.

[29] Marzec, M., Eletto, D., and Argon, Y. (2012) GRP94: An HSP90-like protein specialized for protein folding and quality control in the endoplasmic reticulum, *Biochim. Biophys. Acta, Mol. Cell Res. 1823*, 774-787.

[30] Martinez-Aranda, A., Hernandez, V., Guney, E., Muixi, L., Foj, R., Baixeras, N., Cuadras, D., Moreno, V., Urruticoechea, A., Gil, M., Oliva, B., Moreno, F., Gonzalez-Suarez, E., Vidal, N., Andreu, X., Segui, M. A., Ballester, R., Castella, E., and Sierra, A. (2015) FN14 and GRP94 expression are prognostic/predictive biomarkers of brain metastasis outcome that open up new therapeutic strategies, *Oncotarget 6*, 44254-44273.

[31] Wei, P.-L., Huang, C.-Y., Tai, C.-J., Batzorig, U., Cheng, W.-L., Hunag, M.-T., and Chang, Y.-J. (2016) Glucose-regulated protein 94 mediates metastasis by CCT8 and the JNK pathway in hepatocellular carcinoma, *Tumour Biol. 37*, 8219-8227.

[32] Buc Calderon, P., Sennesael, A.-L., and Glorieux, C. (2018) Glucose-regulated protein of 94 kDa contributes to the development of an aggressive phenotype in breast cancer cells, *Biomed. Pharmacother. 105*, 115-120.
[33] Tramentozzi, E., Ruli, E., Angriman, I., Bardini, R., Campora, M., Guzzardo, V., Zamarchi, R., Rossi, E., Rugge, M., and Finotti, P. (2016) Grp94 in complexes with IgG is a soluble diagnostic marker of gastrointestinal tumors and displays immune-stimulating activity on peripheral blood immune cells, *Oncotarget 7*, 72923-72940.
[34] Zhang, L., Wang, S., Wangtao, Wang, Y., Wang, J., Jiang, L., Li, S., Hu, X., and Wang, Q. (2009) Upregulation of GRP78 and GRP94 and its function in chemotherapy resistance to VP-16 in human lung cancer cell line SK-MES-1, *Cancer Invest. 27*, 453-458.
[35] Fu, Y., and Lee, A. S. (2006) Glucose regulated proteins in cancer progression, drug resistance and immunotherapy, *Cancer Biol. Ther. 5*, 741-744.
[36] Duerfeldt, A. S., Peterson, L. B., Maynard, J. C., Ng, C. L., Eletto, D., Ostrovsky, O., Shinogle, H. E., Moore, D. S., Argon, Y., Nicchitta, C. V., and Blagg, B. S. J. (2012) Development of a Grp94 inhibitor, *J. Am. Chem. Soc. 134*, 9796-9804.
[37] Chavany, C., Mimnaugh, E., Miller, P., Bitton, R., Nguyen, P., Trepel, J., Whitesell, L., Schnur, R., Moyer, J. D., and Neckers, L. (1996) p185erbB2 binds to GRP94 in vivo. Dissociation of the p185erbB2/GRP94 heterocomplex by benzoquinone ansamycins precedes depletion of p185erbB2, *J. Biol. Chem. 271*, 4974-4977.
[38] Schulte, T. W., Akinaga, S., Murakata, T., Agatsuma, T., Sugimoto, S., Nakano, H., Lee, Y. S., Simen, B. B., Argon, Y., Felts, S., Toft, D. O., Neckers, L. M., and Sharma, S. V. (1999) Interaction of radicicol with members of the heat shock protein 90 family of molecular chaperones, *Mol. Endocrinol. 13*, 1435-1448.
[39] Taldone, T., Zatorska, D., Patel, P. D., Zong, H., Rodina, A., Ahn, J. H., Moulick, K., Guzman, M. L., and Chiosis, G. (2011) Design, synthesis, and evaluation of small molecule Hsp90 probes, *Bioorg. Med. Chem. 19*, 2603-2614.
[40] Huck, J. D., Que, N. L. S., Immormino, R. M., Shrestha, L., Taldone, T., Chiosis, G., and Gewirth, D. T. (2019) NECA derivatives exploit the paralog-specific properties of the Site 3 side pocket of Grp94, the ER Hsp90, *J. Biol. Chem.*
[41] Soldano, K. L., Jivan, A., Nicchitta, C. V., and Gewirth, D. T. (2003) Structure of the N-terminal domain of GRP94. Basis for ligand specificity and regulation, *J. Biol. Chem. 278*, 48330-48338.
[42] Moulick, K., Clement, C. C., Aguirre, J., Kim, J., Kang, Y., Felts, S., and Chiosis, G. (2006) Synthesis of a red-shifted fluorescence polarization probe for Hsp90, *Bioorg. Med. Chem. Lett. 16*, 4515-4518.
[43] He, H., Zatorska, D., Kim, J., Aguirre, J., Llauger, L., She, Y., Wu, N., Immormino, R. M., Gewirth, D. T., and Chiosis, G. (2006) Identification of potent water soluble purine-scaffold inhibitors of the heat shock protein 90, *J. Med. Chem. 49*, 381-390.
[44] Kim, J., Felts, S., Llauger, L., He, H., Huezo, H., Rosen, N., and Chiosis, G. (2004) Development of a fluorescence polarization assay for the molecular chaperone Hsp90, *J. Biomol. Screen. 9*, 375-381.